International Journal of Engineering Applied Sciences and Technology, 2021
Vol. 6, Issue 3, ISSN No. 2455-2143, Pages 51-61
Published Online July 2021 in IJEAST (http://www.ijeast.com)

SIMULATION OF DYNAMIC EVENT OF IMPACT USING EXPLICIT 3D FEM MODEL AND VALIDATION BY EXPERIMENT AND CONTACT MODELS

Akshay Mallikarjuna, Dan Marghitu, P.K.Raju
Department of Mechanical Engineering
Auburn University
Auburn, AL, USA

Abstract— **In this study, an optimized method to simulate the dynamic 3D event of the impact of a rod with a flat surface has been presented. Unlike the 2D FEM based contact models, in this study both the bodies undergoing the impact are considered elastic(deformable) and simulation is the dynamic event of the impact, instead of predefined 2D symmetric contact analysis. Prominent contact models and plasticity models to define material properties in ANSYS are reviewed. Experimentation results of normal and oblique impact of the rod for different rods provided the coefficient of restitution. Experimental results of permanent deformation on the base for different impact velocity is derived out of a prominent impact study. The simulation results are in co-relation with experiment and both indentation and flattening models on the coefficient of restitution (COR) and permanent deformation of the base and rod after the impact. Thus, the presented 3D Explicit Dynamic simulation of impact is validated to analyze the impact behavior of the 2 bodies without any predefined assumptions with respect to boundary conditions or material properties.**

Keywords— **Low Velocity Impact, 3D Explicit Dynamic Simulation, Contact Models, Validation, Permanent Deformation, Coefficient of Restitution.**

I. INTRODUCTION

The comparison of the experimental results and the Finite Element Analysis (FEA) of a low velocity impact of sphere and rods have gained attention since the beginning of 21st century. Till date the impact models which are formulated are based on implicit 2D contact models with the predefined contact conditions. Normally the contact models consider either the flat or the hemispherical body under motion as rigid. The models considering the impacting body as rigid are called indentation models and models considering the fixed flat surface under impact as rigid are called flattening models. There are very few models which considered both the impacting body and the surface undergoing the impact as elastic. The present study validates a 3D Explicit Dynamics FEM [24] model using these contact models and experimental results of the impact, so that this FEM model can be used to simulate and analyze more complicated 3D asymmetric systems by dynamic simulation of impact.

Hertz contact theory is the base to study the impact of the fully elastic object. He established a closed form solution for the impact of 2 elastic spheres based on which other theories are formulated. However, Hertz theory is limited to only the elastic phase of the impact, the plasticity involved during the event of impact is not addressed in Hertz theory. Later, the study on indentation to measure the hardness of the material gave the experimental results for the contact studies. The experiment done by Tabor [3] on indentation revealed the physical insight into the surface interactions. Johnson [12] in the mid 90's put forth a model dividing the event of impact as fully elastic and fully plastic phase. His further study [20] demonstrated that the restitution phase of impact will always have a reverse plastic flow rather than the purely elastic recovery, and this was backed by Tabor's experiment. Furthermore, many theoretical models were proposed improving the Hertz theory, but achieving a closed form solution addressing plasticity, instantaneous velocity and instantaneous force was a problem. In the early 90's, Stronge [22],[21] came up with the energy approach to study the event of impact and introduced a new coefficient of restitution based on energy principle. In later 90's with the advent of Finite Element Method (FEM), the study of contact got more interested towards micro-indentation [1] and nano-indentation [18]. Many models were put forth to predict these factors which were unable to solve through traditional closed form theories. Tabors experimental results served as a reference for many FEM models. The early FEM indentation models were based on minimal computational time and effort. Hardy [8] et.al. in 1971, Kral et.al [16] in 1993, and Ogbonna et.al [19] in 1995 studied these indentation models in FEM, their work concentrated on achieving the appropriate mesh and effective computational time for the analysis to validate the

International Journal of Engineering Applied Sciences and Technology, 2021
Vol. 6, Issue 3, ISSN No. 2455-2143, Pages 51-61
Published Online July 2021 in IJEAST (http://www.ijeast.com)

results to Tabor experiments. Mesarvic and Fleck [17] in 1999 studied the Brinell indentation as a part of large computational study. Since the early 2000's more sophisticated models were designed with increased computational power. The models were more robust, and many scholars came up with empirical formulations to predict the contact force, deformation or indentation, and other behaviors of impact based on the simulator results. Yo Komvopoulos [25] developed a new formulation for the indentation of homogeneous and layered material using FEM. Kogut and Komvopoulus (KK model) [14] came up with an interactive approach through FEM simulation for determining the indentation, contact force and plastic deformation of the base. These results are also validated by his experiments. Later Kogut and Elsio (KE model) [13] presented a flattening model with a new empirical formula on elastic-plastic contact of a sphere on a rigid flat. Komvopoulos and Ye [15] were first to model a 3-Dimentional contact analysis of impact with non-homogeneous flat, with accounting the roughness of the surface. Jackson and Green (JG model) [11] in 2004 presented a flattening model, they used the axissymmetric 2D model of elastic-perfectly plastic sphere in friction-less contact with a rigid flat. The resulting numerical data is fitted to capture deformations from purely elastic to fully plastic conditions, and in turn developed a new empirical formulation based on Poisson's ratio, elastic modulus, and yield strength of the material under impact. Brake [5] developed a new model to determine the contact force and the area of contact. He further divides the event of impact into 4 phases i.e., fully elastic, elasto-plastic, fully plastic, restitution phase. In the recent studies, Alcala et al. [2] developed a model to determine the mechanical properties of the material under impact considering the effect of friction and strain hardening rate, and contact radius. Further in 2014 Hamid, Marghitu and Jackson [6],[7] studied all the above stated models and formulated a modified version of JG model to measure the indentation on the impact base, using the experimental and FEM results. Recent studies by Kefie, Jackson [10] and Yang, Green [23] on the contact analysis are focused on the 3D simulations and FEM parametric analysis of line and surface contact rather than point contact. The effect of friction and hardening are studied for specific cases of plane stress and plane strain. These studies are imitated to specific cases and the present study is an attempt towards to generalize and validate the dynamic 3D simulation of the contact.

II. INDENTATION MODELS

A. *Hertzian Contact theory* –

Basic formulation of Hertzian Contact theory (Spherical indenter) of indentation model is described here.

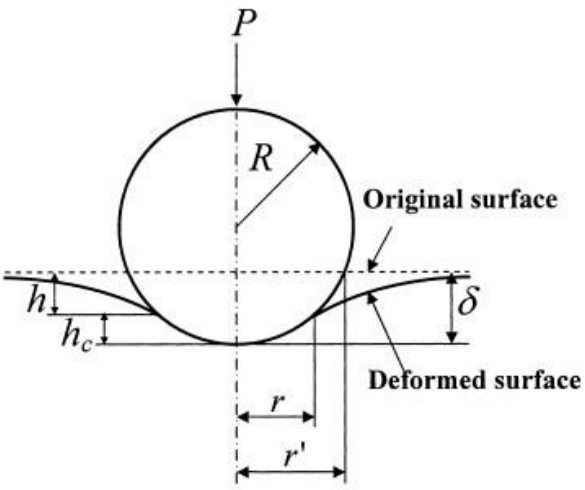

Fig. 1. Schematic illustration of spherical indentation.

The mean contact pressure P_m of the contact is defined as.

$$P_m = \frac{P}{a} \tag{1}$$

where 'a' is contact area and 'P' is the normal load and truncated contact area 'a'' is defined as.

$$a' = \pi(r')2 = \pi\delta(2R - \delta) \tag{2}$$

which is given as a function of radius of the truncated contact area 'r'' and the indentation 'δ' of the rigid sphere on the flat. Based on Hertz theory, the reduced modulus of elasticity is given by.

$$E = \left[\frac{(1-\vartheta_1{}^2)}{E_1} + \frac{(1-\vartheta_2{}^2)}{E_2}\right] \tag{3}$$

where E is the reduced modulus of elasticity. For the elastic phase the indentation δ is.

$$\frac{\delta}{r_1} < 1.78\left(\frac{E}{Y}\right)$$

after which the material starts to yield.

The deformation δ of the flat can be written as a function of contact load and material properties.

$$\frac{P_m}{Y} = \frac{4\sqrt{2}}{3\pi}\frac{E'}{Y}\frac{\delta}{r'} \tag{4}$$

$$\frac{a'}{a} = 2$$

B. *Komvopoulus Kogut Model (KK Indentation Model)*

International Journal of Engineering Applied Sciences and Technology, 2021
Vol. 6, Issue 3, ISSN No. 2455-2143, Pages 51-61
Published Online July 2021 in IJEAST (http://www.ijeast.com)

KK indentation model divides the event of impact as 3 phases: Elastic Phase, Elasto-Plastic phase, and Restitution phase. Elastic phase is governed by Hertz contact theory. Based on the empirical results, and FEM analysis interface between the elastic phase and elastic-plastic phase is formulated as constant ratio between contact pressure and the yield strength of the material (Eq:5) or expressed as critical deformation (Eq:6) at which yielding is initiated.

In the elastic-plastic phase the expression for contact pressure and contact area were derived by using FEM simulation results.

$$\frac{P_m}{Y} = 0.839 + \ln[\left(\frac{E}{Y}\right)^{0.656} \left(\frac{\delta}{r'}\right)^{0.651}] \quad (5)$$

$$\frac{a'}{a} = 2.193 + \ln[\left(\frac{E}{Y}\right)^{0.394} \left(\frac{\delta}{r'}\right)^{0.419}] \quad (6)$$

Further by correlating these 2 expressions a dimensionless contact load is defined as.

$$\frac{P_m}{a'Y} = \frac{0.839 + \ln[\left(\frac{E}{Y}\right)^{0.656} \left(\frac{\delta}{r'}\right)^{0.651}]}{2.193 + \ln[\left(\frac{E}{Y}\right)^{0.394} \left(\frac{\delta}{r'}\right)^{0.419}]} \quad (7)$$

The restitution phase is described as unloading behavior or recovery phase, the plastic or permanent deformation is called the residual impression δ_r. The recovery of the elastic deformation of the material is characterized by the change of the displacement at the center of indentation $E_{R\delta}$, which is defined as.

$$E_{R\delta} = \frac{\delta_i - \delta_r}{\delta_i} \quad (8)$$

where δ_i is the maximum indentation on the base in the event of impact δ_{max}. Also, the ratio of the elastic energy released upon unloading to the total input energy during loading is defined as.

$$E_{RE} = \frac{\int_{\delta_f}^{\delta_i} P(\delta) d\delta}{\int_0^{\delta_i} P(\delta) d\delta} \quad (9)$$

Using the curve fitting for these results obtained from simulation, the ratios are expressed in terms of mechanical properties of the material as shown.

$$E_{R\delta} = 0.591 \left(\frac{E}{Y}\right)^{-0.156} \quad (10)$$

$$E_{RE} = 0.616 \left(\frac{E}{Y}\right)^{-0.176} \quad (11)$$

So, by rearranging the terms we can get the expression for permanent deformation on the impact point of the base.

$$\delta_r = \delta_i [1 - E_{R\delta}] \quad (12)$$

*C. **Brake Indentation Model***

Brake's model formulated contact behavior of indentation by accounting for friction and strain hardening effect. Brake's model divides the impact into elastic phase and elastic-plastic phase. In his study a transitionary function is used to define the behavior of impact with 9 practical assumptions applied to bound the function for one realistic solution. Elastic Phase is again governed by Hertz contact theory, indentation at the point of initiation of yielding is given by.

$$\delta_y = \frac{r}{F(\vartheta)} \left(\frac{\pi \sigma_y}{2E}\right)^2 \quad (13)$$

In the elastic-plastic phase i.e., when $\delta > \delta_y$, nonlinear strain hardening coefficient 'H' and exponent 'n' are used to account for effect of hardness of the material during the event of impact. Contact compliance after the inception of yielding is expressed using the transitionary function.

$$F = \operatorname{sech}\left((1 + n_\epsilon)\frac{\delta - \delta_y}{\delta_p - \delta_y}\right)\frac{4}{3} E\sqrt{r}\, \delta^{\frac{3}{2}} + \left(1 - \operatorname{sech}\left((1 + n_\epsilon)\frac{\delta - \delta_y}{\delta_p - \delta_y}\right)\right) p_0 \pi \frac{a^n}{{a_p}^{n-2}} \quad (14)$$

$p_0 = Hg10^6$ is the contact pressure for a fully developed plastic flow without strain hardening and $H = \left(\frac{2}{H_g} + \frac{2}{H_f}\right)^{-1}$ is the Brinell's Hardness of the material and $n_\epsilon = n - 2$ is strain hardening exponent where 'n' is the Meyer's hardening exponent. a_p is the characteristic contact radius of the plastic regime expressed as.

$$a_p = \left(\frac{3p_0}{4E}\, 2^{n/2}\, \pi\, r^{(n-1)/2}\, \delta_y^{(n-3)/2}\right)^{1/(n-2)} \quad (15)$$

International Journal of Engineering Applied Sciences and Technology, 2021
Vol. 6, Issue 3, ISSN No. 2455-2143, Pages 51-61
Published Online July 2021 in IJEAST (http://www.ijeast.com)

and the indentation at the end of elastic-plastic phase is expressed as.

$$\delta_p = \frac{a^2{}_p}{2R} \tag{16}$$

The restitution or unloading phase is assumed to be elastic in nature and hence is governed by Hertz theory. At the end of loading phase, a deformed radius of curvature r' and permanent indentation δ' is sustained in the body due to plastic deformation. δ' the permanent deformation and r' deformed radius of curvature is expressed as function of maximum deformation δ_m and maximum contact force F_m during the loading phase.

$$\delta' = \delta_m \left(1 - \frac{F_m}{4/3\, E \sqrt{r\delta_m^{3/2}}} \right) \tag{17}$$

similarly, the radius of curvature of unrecoverable indentation is expressed as.

$$r' = \frac{F^2{}_m}{4/3\, E \sqrt{r\delta_m^{3/2}}} \tag{18}$$

III. FLATTENING MODELS

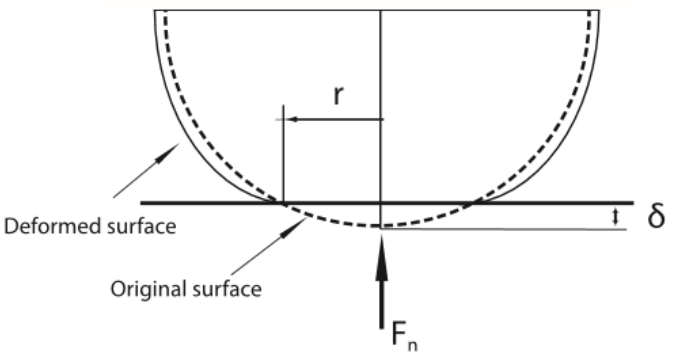

Fig. 2: Schematic illustration of elastic-spherical surface impacting on a rigid-flat

A. Jackson Green Model

The Jackson Green's model uses 2D axisymmetric finite element model of an elastic-perfectly plastic sphere in frictionless contact with a rigid flat. Figure:2 shows the schematic representation of the flattening model. Here the elastic hemisphere is in contact with a flat surface with a static contact load 'F_n'. The event of the contact(compression) is divided into elastic and elastic-plastic regime. The deformation 'δ' is in elastic region until the inception of yielding, the point where material starts to yield is defined as critical interface 'δ_c' of deformation. Jackson Green's Model provided an analytical expression for critical deformation by using the von Mises yield criterion. δ_c is expressed in terms of yield strength of the hemisphere.

$$\delta_c = \left(\frac{\pi C Y}{2E} \right)^2 R \tag{19}$$

C is the yield strength coefficient defined as the ratio of maximum contact pressure to yield strength of the material.

$$C = \frac{P_{oy}}{Y} = 1.295\, e^{0.736\vartheta} \tag{20}$$

P_c is the critical load to initiate yielding during the impact.

$$P_c = \frac{4}{3} \left(\frac{R}{E} \right)^2 \left(\frac{C}{2} \pi\, Y \right)^3 \tag{21}$$

In elastic plastic phase an empirical formula is developed using FEM simulation results of various interfaces of impact with different material properties and spherical geometric parameters. The effect of hardness at the high interface of the impact is isolated by defining a ratio of average pressure H_G to yield strength Y. Thus, the change in the hardness with the amount of contact interface was established. Further fitting those FEM results with Weibull function, an expression relating the mechanical properties with the contact area and deformation is formulated.

$$\frac{H_G}{Y} = 2.84 \left[1 - e^{\left(-0.82(a/R)^{-0.7}\right)} \right] \tag{22}$$

$$\frac{a}{R} = \frac{\pi C e_y}{2} \left[\delta^* \left(\frac{\delta^*}{\delta_t^*} \right)^B \right]^{1/2} \tag{23}$$

Restitution phase is formulated in the further study of the JG model [11] as the model evolved with the analysis of more FEM simulation results using curve fitting models to predict the empirical formula for the plastic deformation δ' and rebound velocity (COR) of the elastic-perfectly plastic sphere.

International Journal of Engineering Applied Sciences and Technology, 2021
Vol. 6, Issue 3, ISSN No. 2455-2143, Pages 51-61
Published Online July 2021 in IJEAST (http://www.ijeast.com)

$$\delta' = \delta_m \left(1.02\left[1 - \left(\frac{\delta_m/\delta_c + 5.9}{6.9}\right)^{-0.54}\right]\right) \quad (24)$$

B. Modified Jackson Green Model

The FEM model developed by Hamid, Jackson and Marghitu [6],[7] called as Modified JG model is also based on the 2D elements with asymmetric condition. Modified JG model has evolved from studies of all the previous indentation and flattening models where one of the bodies under impact was assumed to be rigid. In this model, both the surfaces undergo the impact elasto-plastically. By comparing and correlating with many prominent FEM models and validating with the experimental results, a successful attempt has been made to explain and provide a transition between the indentation and flattening models and predict the contact force, permanent deformation and rebound velocity during impact on both the surfaces. This study follows the same theory of JG model and hence for elastic phase of the impact the expressions remain same for contact force and deformation. For elasto-plastic phase a new term is expressed as the ratio S_y of yield strength of sphere S_{ys} and flat S_{yf}.

$$S_y = \frac{S_{ys}}{S_{yf}}$$

which is used to formulate transitioned normalized hardness expression accounting for change in hardness in both the surface, in turn the contact force and deformation. The restitution phase follows the Hertz theory. The expression given below is for the permanent deformation δ_r and contact P_r force, based on empirical formula to describe the deformation on both the surfaces undergoing the impact.

$$\delta' = 0.8\,\delta_m \left[1 - \left(\frac{\delta_m/\delta_c + 5.5}{6.5}\right)^{-2}\right] \quad (26)$$

where δ_r is the permanent deformation after unloading phase, δ_m is the maximum deformation at the compression phase.

$$P_r = \frac{4}{3} E R'^{0.5} \quad 27)$$

The restitution phase is governed by Hertz theory as in JG model and hence, the expression for deformation and contact load remains same for both bodies. Respective maximum and critical deformation can be used to approximate the permanent deformation on either spherical or flat surface.

IV. FINITE ELEMENT ANALYSIS

The dynamic 3D model of the rod with a spherical-end impacting with a fixed flat is modeled using Explicit Dynamics module under ANSYS-Workbench. The model as shown in Figure 4 is meshed with 3D elements with Lagrangian reference frame.

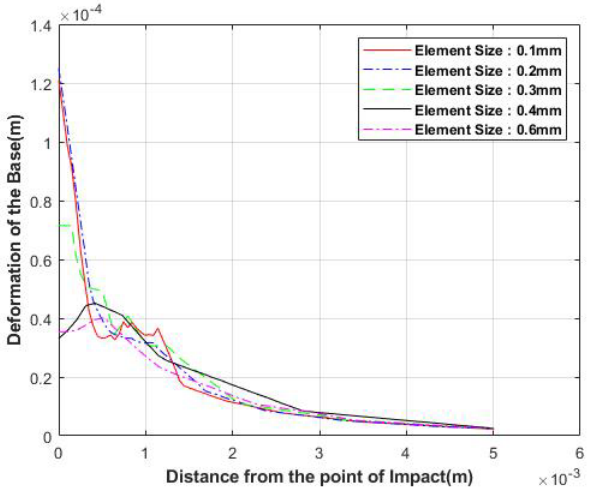

Fig. 3: Max deformation of the base over the contact region for different mesh density

Many simulations with different meshes are carried considering the computational time and to have a consistent result independent of mesh density. The maximum displacement over time of the base under impact for various mesh sizes are shown in Figure3. The abscissa represents the distance from point of impact to the end of contact during the impact and ordinate represents the maximum deformation caused by the impact over time. From the graph as shown in figure 3, it is evident that the maximum displacement response at the contact point is almost convergent for mesh size of 0.002mm. It should be noted that in this convergence study the path result of the displacement over the length of the contact accounts for the discontinuity errors due to lack of sufficient nodes at the contact region. The mesh convergence is achieved with element size of 10^{-5} as shown in Figure 5 within 0.1mm around the vicinity of the impact point both for normal and oblique impact. For the dynamic impact analysis, the time step of the simulation depends on the smallest element and sound wave speed in the material under test. As the event of the impact is in the order of milliseconds a time step of $2 * 10^{-9}$s is used in the simulation. To accommodate the whole event of the impact and sufficient time to plot the rebound velocity the event is simulated for 10 microseconds. The models with different radii and lengths and impact velocities are meshed with 20 to 25 thousand nodes and 100 to 150 thousand elements based on the parameters of the rod. The rod is modeled in such a way that it is 0.001mm away

International Journal of Engineering Applied Sciences and Technology, 2021
Vol. 6, Issue 3, ISSN No. 2455-2143, Pages 51-61
Published Online July 2021 in IJEAST (http://www.ijeast.com)

from the base so that the computational time can be saved in the dynamic analysis. AUTODYNA solver is used for the analysis. Normally in the dynamics simulation mass scaling is used to improve the time efficiency of the computation. Mass scaling is the process where density of the material is artificially increased for the smallest element by which the larger time step can be used and hence lesser the time taken to solve the simulation. But in this impact analysis as the smallest element of the structure is at the point of impact, change in the density of the elements results in change in inertial aspects of the impact. Hence in explicit dynamics simulation of impact we cannot have the luxury of mass scaling to reduce the computation time. The computation time is between 6-7hr on a computer with i7 processor with 16GB RAM. More than 200 different cases of simulations are performed. Results are analyzed and correlated with the mentioned prominent models of impact mechanics and experimental results. The time step for all the dynamic analysis is in the order of 10^{-8}s as the event of impact is in the order of 10^{-5}s. The range of material and geometric parameters modeled in these simulations are in exact co-relation with those used in the experiments and mentioned contact models.

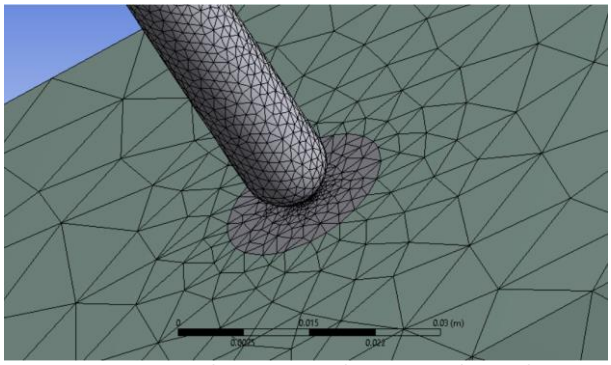

Fig. 4: FEM model of the impact of a rod on a flat surface

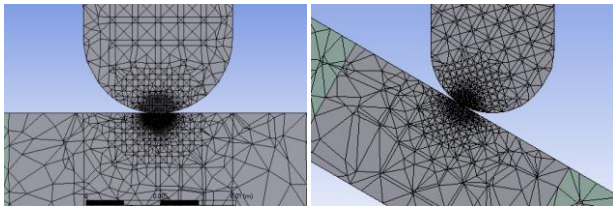

Fig. 5: Cross-sectional view of the mesh for the normal and oblique impact of the rod

In the explicit dynamics, for the simulation of impulsive loading as in case of impact or detonation the material behavior in the plasticity zone is affected by type of loading and strain rate and temperature. For the computation of these systems, along with the elastic properties of the material, plastic and failure properties of the materials are defined by many formulations. Each formulation of the material hardening properties by these models address the change in properties of the material at the specific scenario. Formulations used in the ANSYS Workbench to define the plastic properties of the materials are briefly described here.

Bi linear, multi linear and nonlinear isotropic hardening is where after initial yielding point the stress as a function of plastic strain can be expressed as a linear slope (Tangent modulus) or as a set of experimental values of stress for a respective plastic strain or as an exponent of strain (Power Law). These hardening laws are generalized plasticity formulations which does not account for change in the material behavior for strain rates or impulsive loads. These properties can be used if there are experimental values of stress strain plots for the given strain rate.

One of the popular plasticity studies for the computation of high velocity impact and stress flow in the materials for the thermal loads is Johnson-cook strength model. This constitutive model is used for computation of flow stress accounting the effects of strain hardening, strain hardening rate and thermal softening.

Cowper Symonds strength and Zerilli Armstrong strength models are in-principle follow Johnson-Cook model with the different modifications. Cowper Symonds strength model is normally used in the simulation of metal cutting, which dictates the formation of the chips and hardening of the material in the process. According to Zerilli and Armstrong, materials have its own constitutive behavior based on its molecular structure type like in Body-centered or Face centered, which will have a distinctive dislocation characteristic. Another popular study of plasticity is Steinberg Guinan strength model used to model the shock wave in the metals as a result of very high velocity impact. In this elastic-plastic constitutive model, the dependency of shear modulus of the metal on the rate of change in pressure and temperature is addressed.

For our study the material property was defined using all of these models and simulated low velocity impact which is our point of interest. For the Bilinear, non-linear or the power law hardening models the results of the deformation and rebound velocity are not consistent with the other contact models and experimental results. As the material property given in these models are not accurate and will not account for the strain rate. Cowper Symonds Strength and Zerili Armstrong Strength model parameters were not experimentally calculated, and approximated values of those parameters did not provide comprehensive results. These studies were not formulated to account impact analysis. Even though the Steinberg Guinan's strength model is formulated to facilitate the computation of impact analysis, this model in particular deviates from the experimental results for low velocity impacts. So, for our study the Johnson-Cook strength model is used to define the elastic-plastic properties of the metals we are testing for impact behavior.

Johnson − Cook Strength

International Journal of Engineering Applied Sciences and Technology, 2021
Vol. 6, Issue 3, ISSN No. 2455-2143, Pages 51-61
Published Online July 2021 in IJEAST (http://www.ijeast.com)

Johnson-Cook strength parameters are used in this low velocity impact study to account for plasticity in the material. In this model the flow stress is expressed as follows:

$$\sigma = (A + B\,\epsilon^{n})(1 + C\,\ln(\epsilon^{*}))(1 - T^{m}) \quad (28)$$

Where σ is the equivalent stress, A is the initial yield stress, B is the hardening constant, ϵ is the plastic strain, n is the strain hardening exponent, C is the strengthening coefficient of strain rate, ϵ^{*} is the normalized effective plastic strain and m is thermal softening coefficient. These parameters can be obtained by true stress strain plot [4] [9] of the materials at different strain rates. Table [1] lists the material properties of rod and base used in this study based on Johnson-Cook-strength model.

Properties	Rod (AISI 201)	Flat (AISI 1010)
ρ	7800 kg/m^3	7830 kg/m^3
E	212 GPa	200 GPa
ν	0.28	0.28
A	750 MPa	300 MPa
B	1793 MPa	633 MPa
n	0.523	0.13
C	0.014	0.014

Table-1: Material properties of rod and base

V. EXPERIMENTATION AND MOTION ANALYSIS

The experimental setup is shown in Fig.6. The impacting base is fixed on a rigid table. A robotic arm is used to drop the rod vertically from different heights. Two lights, 1000W each, have been used to capture a clear image during the impact. A high-speed camera capable of recording with 10,000 frames per second (fps) has been used to capture the motion of the rod before, during and after the impact. After each impact, the event of the impact has been recorded and measured. 10 clear trails of each rod impact have been recorded and analyzed with motion analysis to make sure of having a consistent result. Using this setup, both normal and oblique impact analysis is done. The whole event of the impact is captured and recorded by the high-speed camera.

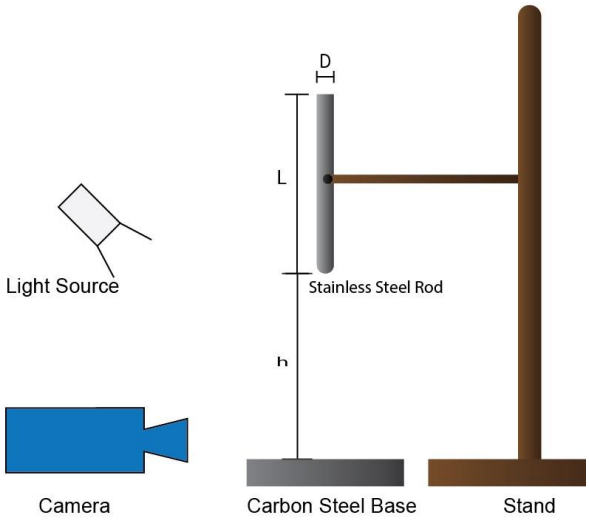

Fig. 6: Schematic representation of experimental setup

Each recorded clip is trimmed to get at least 300 frames close to the point of impact of rod, and each frame contained 512*512 pixels. A motion analysis software is used to calibrate and measure the position of the rod over time. To calculate the velocity of the rod before and after the impact, a certain point on the rod has been tracked. Fig 8 shows the normal impact of a rod and tracking of a point. The red dot indicates the tracker marks as the rod moves. The motion of the rod for before impact and after the impact has been accurately captured. These motion frames are calibrated to get actual displacement profile of the impact over time. The displacement plot of the contact point is used to calculate the velocity of the rod, as shown in Figure 9. The velocities have been calculated from the slopes of the displacement plot before and after the impact, respectively.

International Journal of Engineering Applied Sciences and Technology, 2021
Vol. 6, Issue 3, ISSN No. 2455-2143, Pages 51-61
Published Online July 2021 in IJEAST (http://www.ijeast.com)

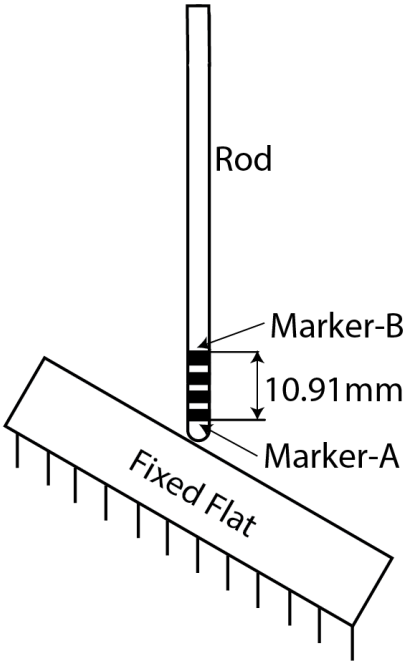

Fig. 7: Oblique impact of rod 2

Fig. 8: Tracking the Normal impact of rod 2

VI. RESULTS AND COMPARISON

A. Comparison of Coefficient of Restitution

The first step in the process of validation of the FEM simulation was done by comparing the simulation and experimental results of coefficient of restitution of 3 different rods dropped from the same height of 0.8m. The properties of the rod and base are described in the section of plasticity models in Table 1. Table-2 shows the dimensions of the rods subjected to impact study. Table-3 is the comparison of experimental results to simulation results of COR of the rod. In the simulation of the impact the direct results of the velocity of the rod after the impact is subjected to lot of variation because of the vibration and shock waves in the rod.

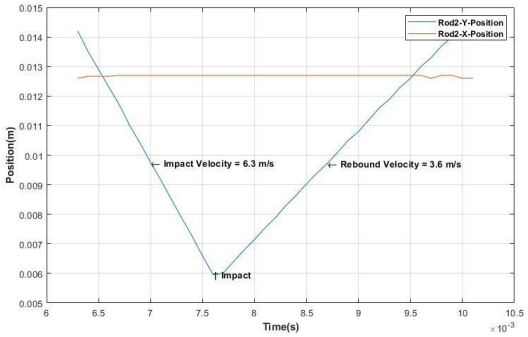

Fig. 9: Displacement plot of tip of the rod 2

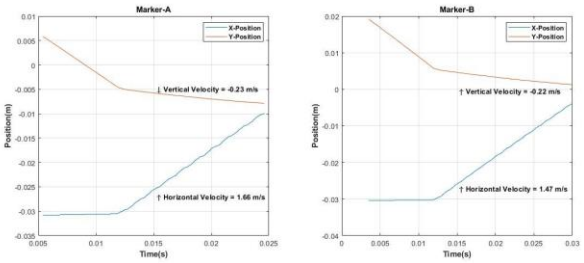

Fig. 10: Displacement plot of 2 markers on rod-2 impacting at 30 degrees

The velocity measured at each node at a given time is different across the length of the rod. Even the average nodal velocity of the whole rod has quite a significant deviation between maximum and minimum value of velocity at any given time. To minimize this deviation, the velocity is measured as slope of the deformation of the whole rod. Thus, this deviation of velocity is averaged over the time after the contact rather than instant velocity given by the velocity probe. From these results it is evident that for the same impact velocity irrespective of rod dimensions the simulation results are in correlation with experimental results. The experimental results of the COR are lower than the simulation results by less than 10 percent. This can be explained as a factor of surface roughness and friction during the impact which is not accounted in the FEM simulation. Comparing the results of COR with the experiment validates the basic mesh convergence and the basic energy balance between the contact bodies. To further validate the results, a similar study was done with oblique impact of the rod. The rod-2 as mentioned in the Table-2 was subjected to oblique impact with different angle and the same system is modeled and simulated. Figure 10 shows the displacement plot of 2 different points on rod-2 impacting at an angle of 30 degrees to the base. These tacking points are denoted as marker A and marker B in the Figure 10, V_A and V_B are the resultant radial velocity of the points respectively. Angular velocity ω of the rod is calculated by Eq29. Table-4 depicts the comparison of angular velocity of the rod between the experiment and simulation for different angles of impact. As both in the experimental results and

International Journal of Engineering Applied Sciences and Technology, 2021
Vol. 6, Issue 3, ISSN No. 2455-2143, Pages 51-61
Published Online July 2021 in IJEAST (http://www.ijeast.com)

explicit dynamic simulation results, the COR is subjected to variations this cannot be the primary method to validate or to analysis the impact behavior. Further validation is needed for the simulation with respect to the deformation of the base and the rod during the impact.

$$\omega = \frac{V_A - V_B}{Distance\ between\ marker\ A\ and\ B} \qquad (29)$$

	Diameter(m)	Length(m)
Rod-1	0.0096	0.190
Rod-2	0.00640	0.19
Rod-3	0.00475	0.2

Table 2.: Dimensions of the rods used in the study

Rod	COR	
	Experiment	FEM
1	0.406 ±0.012	0.463
2	0.420±0.005	0.485
3	0.559±0.008	0.602

Table 3.: COR of the rod undergoing normal impact

Angle of impact	Angular Velocity (rad/sec)	
	Experimental	Simulated
45°	21.5±0.002	22.07
30°	16.8±0.004	16.73
15°	9.6±0.005	10.12

Table 4.: Experimental and simulation results of angular velocity after impact

B. Comparison of Permanent Deformation of the Base

In the next step, a prominent study in the impact of the rod was taken as a reference to obtain the experimental data of rod impacting a base and the same model was simulated. The experimental results are taken from a reference paper [6] which is a study done by one of the present authors of this paper. In this paper a rod of stainless steel (AISI 201) and base of Carbon steel (AISI 1070) whose material properties are the same as described in our study is tested for impact over different drop heights. The permanent deformation and kinematic coefficient of restitution is measured using a similar motion analysis. The same research is extended in this study to validate our 3D explicit dynamics simulation with these experiments.

Figure 11 compares the experimental data and simulation results of permanent deformation of the base when a rod of 300mm length and 9mm diameter with a spherical end impacts a surface with different drop heights. The results of permanent deformation of the simulation are in good correlation with the experimental and contact model results.

From the graph it is evident that the results of simulation are in correlation with the experiment and contact models. From the graph it is evident that the permanent deformation of the base is in co-relation with the contact models. Especially with the modified Jackson Green model the results are closer to the experimental results. The presented dynamic simulation method accounts for deformation on both the bodies undergoing impact which is the main principle on which the modified Jackson green model was formulated and hence the co relation is justified. Figure 12 shows the reaction force with respect to the deformation of the base for different drop heights of impact. Reaction force F^r can be calculated from the nodes where boundary conditions are defined. It is the response of the structure for all the loads acting on it. In a basic sense reaction force is the difference between the summation of elastic static, F_e^k damping F_e^c and inertial F_e^m loads to the applied loads F^{nd} as shown in the equation (30).

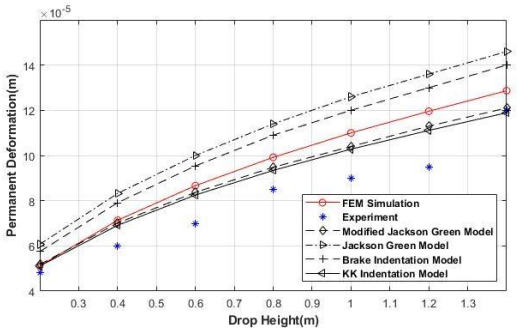

Fig. 11: Comparison of simulation results of permanent deformation of the rod with the reference paper results

$$F^r = -\sum_{e=1}^{N}[F_e^k + F_e^c + F_e^m] - F^{nd} \qquad (30)$$

Close observation of this graph shows for the linear progression of impact velocity that the deformation tends to reduce as the effect of higher strain hardening for higher strain with the increase in impact velocity.

International Journal of Engineering Applied Sciences and Technology, 2021
Vol. 6, Issue 3, ISSN No. 2455-2143, Pages 51-61
Published Online July 2021 in IJEAST (http://www.ijeast.com)

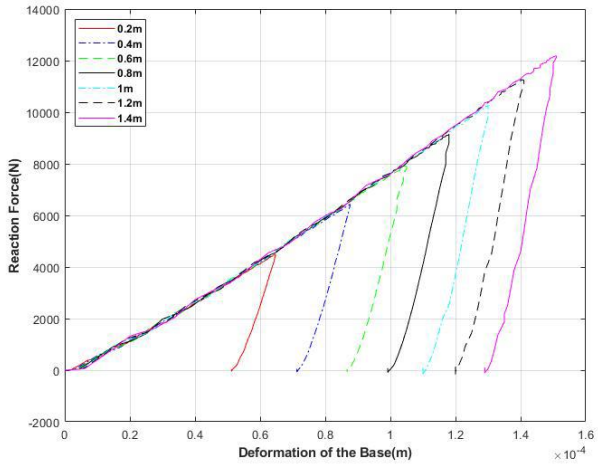

Fig. 12: Force reaction v/s deformation of base for different drop heights of impact

C. *Permanent deformation of the rod*

An attempt is made to determine the permanent deformation on the rod, which is not directly available in the solutions of the analysis. ANSYS simulation measures the deformation as the change in position of the node during the simulation. But when the body without boundary condition or constrains undergoes a displacement, that is considered as the deformation in the results of the simulation. In our case of impact analysis, the rod undergoes both free body motion and also deformation during the impact. One convenient way to separate the factor of free body motion from the deformation plot is to find the difference in the displacement of rod at any point on the rod from the impact point. But the resulting deformation of the rod will be inconsistent as the rod undergoing the impact will have compression and vibrations along the process of impact. This problem can be solved by measuring the plastic strain on the nodes near the point of impact as shown in the Figure 13. Deformation of the rod is obtained by difference in the displacement of the node at point of impact to the nearest node to the impact point at which the plastic strain is 0.

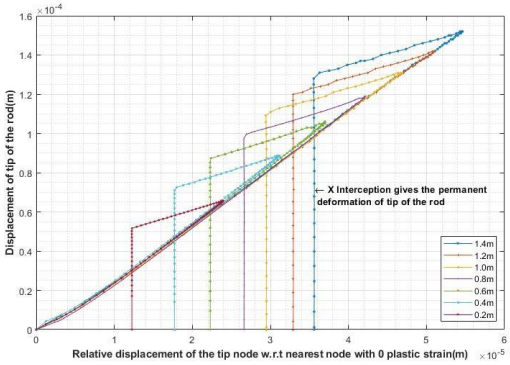

Fig. 13: Measuring the permanent deformation of the rod by relative displacement of tip of the rod

The plot of this displacement also shows the impact phases of compression and restitution. After the contact is ended the plot is parallel to y axis, thus representing no relative displacement between the nodes and hence that should be the permanent deformation on the rod which cannot be recovered. Figure 14 depicts the permanent deformation of the rods for different drop heights.

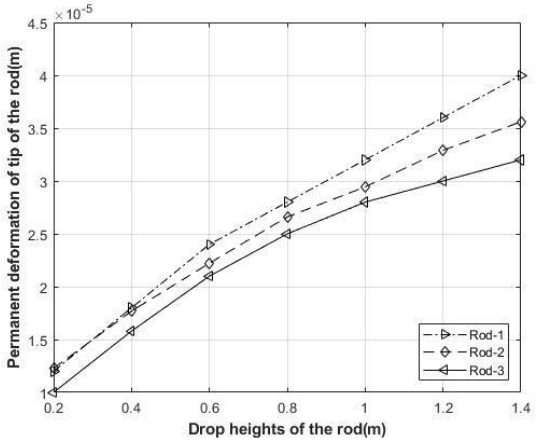

Fig. 14: Permanent deformation of the rod for different drop heights of impact

VII. CONCLUSION

In this study the impact models are simulated using 3D modeling and the dynamic event of the impact is analyzed by using explicit dynamic solver. This method of 3D dynamic simulation has been validated by experiment and contact models. The first step in the validation is the comparison of experimental results on COR of normal impact and angular velocity of the oblique impact. In the second step from the correlation between the simulation and a reference study [7] of impact of the rod on permanent deformations of the base, it is evident that the result presented in the reference study further validates the presented simulation on analysis of deformation during and after event of impact. This same model is also compared with the prominent indentation and flattening contact models. From that comparison it evident that the simulation results are in close agreement to modified Jackson Green model, as the principle under modified Jackson Green model study also considers deformation on both the bodies undergoing impact. Further, the effect of strain rate is shown by the progression of permanent deformation with the impact velocity. With these comparisons it can be inferred that the 3D explicit dynamics analysis presented in this study is valid for the impact analysis of the spherical end on a flat and hence the same method technique can be used to study more complicated models without redoing the validation of that system with any empirical data or mathematical models. A method to determine

the deformation of the rod undergoing impact is presented. This study can be further extended to validate the deformation on the rod with the experiments.

VIII. REFERENCES

[1] Varshneya Arun and D.J. Strange Finite element simulation of micro indentation on aluminum. *Journal of Materials Science*, 36(8):1943–1949, Apr 2001.

[2] J. Alcala and D. Esqu´ e-de los Ojos. ´ Reassessing spherical indentation: Contact regimes and mechanical property extractions. *International Journal of Solids and Structures*, 47(20):2714 – 2732, 2010.

[3] A.G. Atkins and D. Tabor. Plastic indentation in metals with cones. *Journal of the Mechanics and Physics of Solids*, 13(3):149 – 164, 1965.

[4] Eren Billur and Muammer Koc¸. Formability of austenitic stainless steels under warm hydroforming conditions. *Transactions of the North American Manufacturing Research Institution of SME*, 37, 01 2009.

[5] M.R.W. Brake. An analytical elastic plastic contact model with strain hardening and frictional effects for normal and oblique impacts. *International Journal of Solids and Structures*, 62:104 – 123, 2015.

[6] Hamid Ghaednia, Dan B. Marghitu, and Robert Jackson. Predicting the permanent deformation after the impact of a rod with a flat surface. *Journal of Tribology*, 137:011403, 10 2014.

[7] Hamid Ghaednia, Dan B. Marghitu, and Robert Jackson. Predicting the permanent deformation after the impact of a rod with a flat surface. *Journal of Tribology*, 137:011403, 10 2014.

[8] C. Hardy, C. N. Baronet, and G. V. Tordion. The elasto-plastic indentation of a half-space by a rigid sphere. *International Journal for Numerical Methods in Engineering*, 3, 1971.

[9] Shao Hsia and Yu-Tuan Chou. Fabrication improvement of cold forging hexagonal nuts by computational analysis and experiment verification. *Mathematical Problems in Engineering*, 2015:ID 835038, 12 2015.

[10] A.V. Sobolev, M.V. Radchenko. Use of Johnson Cook plasticity model for numerical simulations of the SNF shipping cask drop tests. Nuclear Energy and Technology, Volume 2, Issue 4, 2016, Pages 272-276, ISSN 2452-3038, https://doi.org/10.1016/j.nucet.2016.11.014.

[11] Robert Jackson, Itti Chusoipin, and Itzhak Green. A finite element study of the residual stress and deformation in hemispherical contacts. *Journal of Tribology*, 127:484, 07 2005.

[12] K. L. Johnson. The correlation of indentation experiments. *Journal of Mechanics Physics of Solids*, 18:115–126, April 1970.: 10.1016/0022-5096(70)90029-3

[13] Etsion I. Kogut, L. Elastic-plastic contact analysis of a sphere and a rigid flat. *Journal of Applied Mechanics*, 8 2002. 110.1115/1.1490373

[14] L. Kogut and K. Komvopoulos. Analysis of the spherical indentation cycle for elastic–perfectly plastic solids. *Journal of Materials Research*, 19(12):3641–3653, 2004.

[15] K. Komvopoulos and N. Ye. Three-dimensional contact analysis of elastic-plastic layered media with fractal surface topographies. *Journal of Tribology-transactions of The Asme J TRIBOL-TRANS ASME*, 123, 07 2001.

[16] Komvopoulos K. Bogy D. B. Kral, E. R. Elastic-plastic finite element analysis of repeated indentation of a half-space by a rigid sphere. *Journal of Applied Mechanics*, 1993.

[17] Sinisa Mesarovic and Norman Fleck. Spherical indentation of elastic–plastic solids. *Proceedings of The Royal Society a Mathematical Physical and Engineering Sciences*, 455:2707– 2728, 07 1999.

[18] SIVA NAGA VENKATA RAVI KIRAN KURAPATI. Elasticplastic indentation deformation in homogeneous and layered materials: Finite element analysis. 03 2019.

[19] N Ogbonna, Norman Fleck, and Alan Cocks. Transient creep analysis of ball indentation. *International Journal of Mechanical Sciences*, 37:1179–1202, 11 1995.

[20] A. Renger. Johnson, k. l., contact mechanics. cambridge etc., cambridge university press 1985. xii, 452 pp., £ 17.50 p/b. isbn 0521347963. *ZAMM - Journal of Applied Mathematics and Mechanics / Zeitschrift fur Angewandte Mathematik und¨ Mechanik*, 69(7):214–214, 1989.

[21] W. J. Stronge. Energy dissipated in planar collision. *Journal of Applied Mechanics*, 1992.

[22] W. J. Stronge and William Johnson. Rigid body collisions with friction. *Proceedings of the Royal Society of London. Series A: Mathematical and Physical Sciences*, 431(1881):169– 181, 1990.

[23] Huaidong Yang and Itzhak Green. Fretting Wear Modeling of Cylindrical Line Contact in Plane-Strain Borne by the Finite Element Method. *Journal of Applied Mechanics*, 86(6), 04 2019. 061012.

[24] Zeng Qingliang Yang, Yang. Contact response analysis of vertical impact between elastic sphere and elastic half space. *Journal of Shock and Vibration*, 2018.

[25] Komvopoulos K. Ye, N. Indentation analysis of elastic-plastic homogeneous and layered media: Criteria for determining the real material hardness. *Journal of Tribology*, 2003.